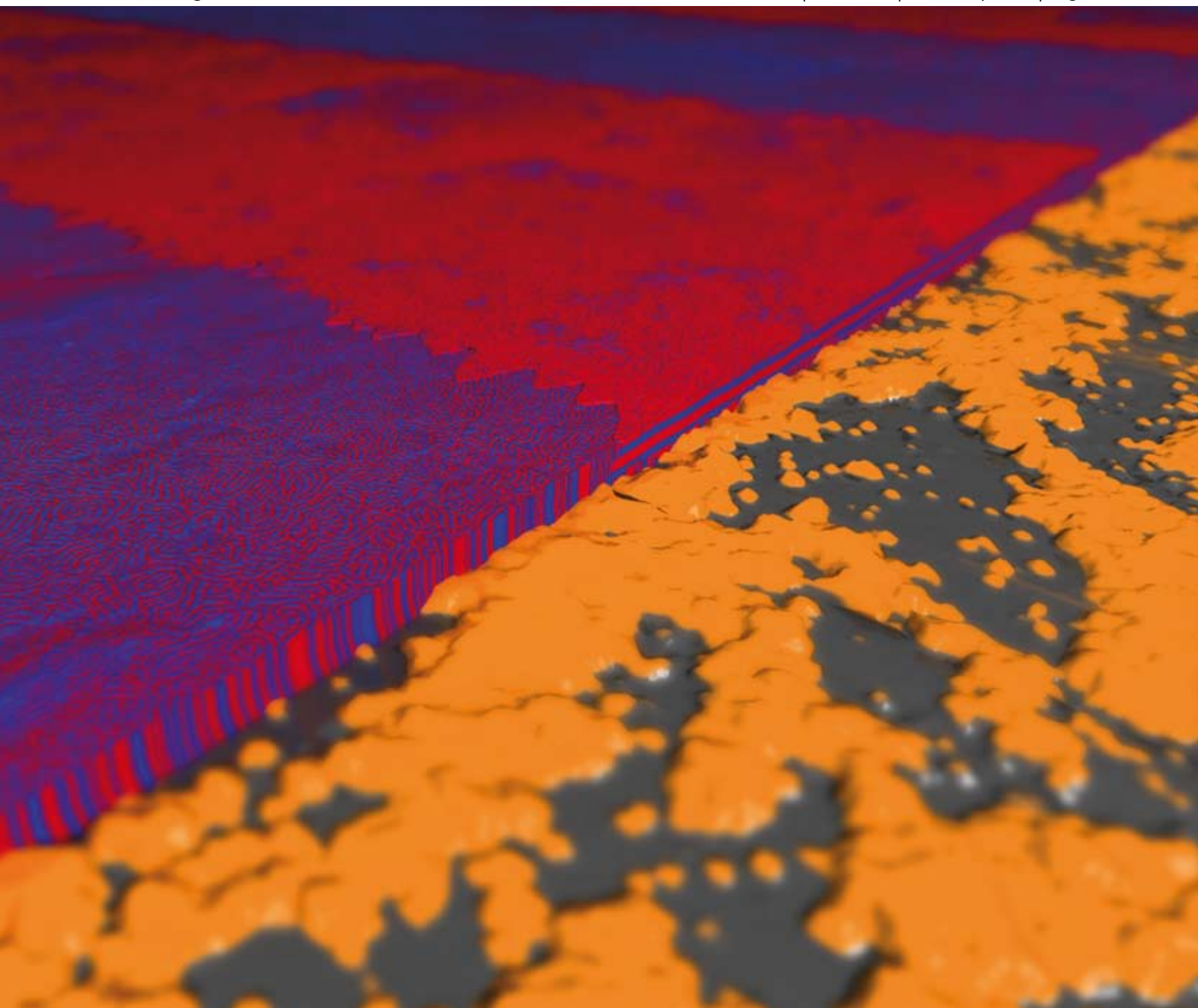


Soft Matter

www.softmatter.org

Volume 5 | Number 3 | 7 February 2009 | Pages 481–692



ISSN 1744-683X

RSC Publishing

PAPER

Alamgir Karim *et al.*
Disordered nanoparticle interfaces for
directed self-assembly

REVIEW

R. G. M. van der Sman
and A. J. van der Goot
The science of food structuring

Disordered nanoparticle interfaces for directed self-assembly†

Kevin G. Yager,^a Brian C. Berry,^a Kirt Page,^a Derek Patton,^a Alamgir Karim^{*a} and Eric J. Amis^b

Received 12th August 2008, Accepted 15th October 2008

First published as an Advance Article on the web 17th November 2008

DOI: 10.1039/b813970a

Self-assembly is a promising route for controlling the nanoscale structure and material properties of coatings, yet it remains difficult to control the microstructure of these systems. In particular, self-assembling materials typically have complex and delicate energy landscapes, which are sensitive to defects, making it difficult to control morphology or orientation. We present a simple and robust strategy for modulating the film-substrate interaction, which can bias the self-assembly energy landscape and thus enforce a desired microstructure. The technique uses nanoparticles with tunable surface energy to generate a rough interface with controlled properties. The intentionally disordered interface is tolerant to variation in substrate preparation. We apply this technique to block-copolymer lamellae, and demonstrate a remarkable thickness-dependence of the induced orientation, consistent with theoretical predictions. The simultaneous control of substrate energy and topography enables expression of the vertical lamellae state without rigorous control of the preparation conditions. We measure an 8-fold increase in surface energy tolerance compared to flat substrates.

Introduction

Coatings find widespread application, including for consumer products, microelectronics, and biomedical implants. Greater control of a coating's microstructure, and of the surface-expression of chemical components, could enable a wide range of novel applications. Directed self-assembly is a possible route to controlling the material properties of coatings, but in general it can be difficult to obtain the desired structure. Self-assembling systems frequently exhibit a variety of morphologies and orientations, with complex energy landscapes determining the preferred state for any particular assembly condition. While this rich phase behavior is central to the usefulness of self-assembling systems, it can also impose stringent preparation requirements for obtaining the desired morphology and domain orientation. Conversely, industrial applications typically require simple, low-cost, robust, and defect-tolerant assembly strategies. We present a general approach for directed self-assembly, based on rough nanoparticle-coated substrates. Importantly, the biasing of self-assembly appears to be relatively insensitive to the details of the substrate preparation.

Block-copolymers (BCPs) micro-phase separate during annealing due to incompatibility between the blocks. This leads to a rich phase behavior,¹ making them ideal models for self-assembly. Symmetric diblock-copolymers form a lamellar morphology, with an intrinsic equilibrium period, L_0 , based on the number or mass average molecular mass. In thin films, these lamellae orient with the sheets parallel to the substrate interface. This is due primarily to preferential wetting at both interfaces: one block will exhibit an energetic preference for the substrate

interface, and one block will exhibit an energetic preference for segregating to the free surface. The geometric constraint of the flat substrate also encourages this horizontal alignment. For film thickness values that are commensurate with the lamellae period, L_0 , the film surface will be flat. In the case of symmetric wetting (the same block has an energetic preference for the substrate interface and the free surface), the commensurate condition occurs for any thickness equal to nL_0 , where n is an integer. For asymmetric wetting (a different block wets the substrate and free surface), commensurability is achieved for any thickness $(n + \frac{1}{2})L_0$. At incommensurate thicknesses, the film surface deforms in order to relieve the stress of a non-equilibrium lamellar period (so-called 'islands and holes'). Because of these factors, it is generally difficult to induce BCP lamellae to orient with the sheets perpendicular to the substrate interface. Techniques used to achieve this orientation of lamellae include: application of electric fields to confined films;²⁻⁴ lithographically-defined chemical patterns;^{5,6} carefully tuning substrate surface energy to be 'neutral' with respect to the diblock wetting;⁷⁻⁹ mixing with nanoparticles;^{10,11} and increasing substrate roughness to a critical level, thereby inducing the vertical orientation due to energetically unfavourable distortions in horizontal lamellae.¹²⁻¹⁴ However, most of these techniques have stringent preparation requirements, and may not be sufficiently simple and robust for widespread low-cost industrial application. For instance, eliminating preferential wetting by tuning substrate chemistry is effective for only a narrow range of substrate energies, thus requiring optimization and strict preparation conditions. Additionally, these techniques may not be generalizable to a wide range of self-assembling systems (e.g., some systems may respond to interfacial energy whereas others may respond to interfacial topography).

Experimental

Colloidal silica nanoparticles (diameter 20 nm, 30% mass fraction suspension in methyl isobutyl ketone (MIBK)) were

^aPolymers Division, National Institute of Standards and Technology, Gaithersburg, MD, USA. E-mail: alamgir.karim@nist.gov

^bMaterials Science and Engineering Laboratory, National Institute of Standards and Technology, Gaithersburg, MD, USA

† Official contribution of the National Institute of Standards and Technology; by acceptance of this article, the publisher and/or recipient acknowledges the US Government's right to retain a nonexclusive, royalty-free license in and to any copyright covering this paper.

obtained from Nissan Chemical Industries, Ltd.¹⁵ Surface modification of silica nanoparticles was carried out according to a modified procedure reported by Savin and coworkers.¹⁶ The nanoparticle dispersion was dried over anhydrous MgSO₄ and filtered. n-Propyldimethylchlorosilane (3 mL) was added dropwise *via* a syringe to the nanoparticle dispersion. The reaction mixture was stirred overnight at 50 °C and allowed to cool to room temperature before adding 6 mL of 1,1,1,3,3,3 hexamethyldisilazane (HMDZ). The reaction was stirred at room temperature for 3 h, and then heated to 50 °C for 8 h. The white precipitate formed upon the addition of HMDZ was removed *via* centrifugation. The orange dispersion was precipitated *via* dropwise addition into a methanol:water mixture (4:1 volume fraction). The particles were centrifuged and the supernatant decanted. The recovered particles were then dissolved in THF and precipitated in the methanol:water mixture. This procedure was repeated 3 times. The particles were then dried at 70 °C overnight under vacuum, producing a fine yellowish powder.

Substrates were polished Si wafers cleaned using warm piranha solution (mixture of 30% volume fraction H₂O₂ and concentrated H₂SO₄ in a 1:3 volume ratio) for 20 min. **Caution:** piranha solution is a powerful oxidant and reacts violently with organics. The silica nanoparticles were cast onto the Si substrates by spin-coating from chloroform solutions. The particle coverage depends on solution concentration and more weakly on spin-coating velocity. The results in this paper were achieved by spin-casting a 0.04% solution (mass fraction) of nanoparticles in chloroform at 126 rad/s for 30 s, which creates partial substrate coverage with high-roughness (rms roughness 10 nm, as measured by AFM). We characterized the hierarchical roughness using 2D areal coverage (51%), the fractal dimensions of the nanoparticle islands boundary was measured using the perimeter-area method¹⁷ (1.44 ± 0.01), and the fractal dimensions of the surface topography using a box-counting method¹⁸ (2.70 ± 0.09). Samples with gradients in nanoparticle surface energy were generated by accelerating the sample beneath a linear UV light-source.¹⁹ Samples for SANS were lightly oxidized by placing in a UV-ozone chamber for 60 s, which produces a static contact angle with water of $\approx 35^\circ$.

The diblock-copolymer was symmetric poly(deuterated-styrene-*block*-methyl methacrylate) (dPS-PMMA), with a molar mass of 62.6 kg/mol (29.5 kg/mol styrene and 33.1 kg/mol methyl methacrylate), and polydispersity index ≈ 1.14 (Polymer Source, Inc.). Thin films were cast from toluene, using either spin-coating (mass fraction 1.5% solution; 100 rad/s to 210 rad/s, depending on desired thickness, for 45 s) or flow-coating (mass fraction 3% solution, 8 mm/s to 40 mm/s sweep speed, depending on desired thickness). Combinatorial samples with a gradient in thickness were prepared using the flow-coating acceleration technique,²⁰ with a blade height of 200 μm , an acceleration of 1 mm/s² to 10 mm/s² (depending on desired thickness range), and 3% (mass fraction) BCP solutions. The BCP films, coated onto silica nanoparticle substrates, were heated in a vacuum oven at 165 °C to anneal the films, and allow the system to micro-phase separate.

Surfaces were imaged using atomic force microscopy (AFM) in the intermittent contact ('tapping') mode of an Asylum MFP3D instrument. The images were segmented by software methods into regions of parallel and perpendicular lamellae.

Segmentation analysis was performed in the IGOR Pro (WaveMetrics) programming environment, using the phase and amplitude AFM images (both of which gave comparable results). The images (512 \times 512 pixels) were flattened (1st-order polynomial) and segmented by calculating local absolute gradients, and using a threshold to differentiate between regions with large absolute gradients (indicative of small-scale patterns arising from perpendicular lamellae) and regions with shallow gradients (indicative of flat parallel lamellae). Similar procedures have been previously used to generate maps of BCP cylinder orientations.²¹ The fraction of vertical lamellae (versus horizontal lamellae), f_v , was calculated based on the relative segmented areas in the images. This segmentation introduces a standard uncertainty of $\pm 3\%$, based on the standard deviation of repeated measurements conducted at the same film location. Film thickness was measured by AFM scratch-height analysis. The reported thicknesses are the total film thickness, including the BCP film, and the underlying nanoparticle layer (which adds, statistically ≈ 12 nm to the overall thickness).

Small-angle neutron scattering (SANS) experiments were performed using the NG7-SANS instrument at the NIST Center for Neutron Research, using an incident neutron beam of wavelength $\lambda = 0.8$ nm ($\Delta\lambda/\lambda = 0.11$). Scans were performed as a function of sample rotation angle in the range -86° to $+86^\circ$. The scattering intensities in the direction of the rotation vector should be invariant with sample rotation, and were used to normalize the intensity of the data. The normalized data was rotated into a coordinate system aligned with the sample (the z -axis points along the normal of the thin film, and the sample lies in the x - y plane)

Results and discussion

In order to address the challenge of directing self-assembly in a general and robust way, we investigated controlling the film-substrate interaction by using tunable nanoparticles, so as to bias self-assembly towards the desired morphology and orientation. Fig. 1a shows a schematic of the 20 nm silica nanoparticles used in this work. The nanoparticles have been decorated with a propyl ligand. This organic coating was chosen because it can be easily oxidized by exposure to ultraviolet light (UV), which generates ozone and atomic oxygen that convert the terminal hydrophobic groups (CH₂, CH₃) into hydrophilic groups (CH₂OH, COOH, etc.). By controlling the exposure time, the surface energy of the nanoparticles can be controlled in a simple and precise way. Specifically, a complete nanoparticle layer is hydrophobic (water contact angle, $\theta_w = 117^\circ \pm 2^\circ$, based on standard deviation of repeated measurements²²), but UV/ozone treatment can convert this to a fully hydrophilic layer ($\theta_w < 10^\circ$), or to any intermediate surface energy.¹⁹ Fig. 1b shows a silicon surface with nanoparticles cast from dilute solution (mass fraction 0.04%), where casting conditions have been selected so as to create a high-roughness, pseudo-fractal surface topography. The ability to independently control interfacial properties—surface coverage *via* casting conditions, roughness *via* nanoparticle size selection, and interfacial energy *via* oxidation—enables optimization for a given system.

To demonstrate biased self-assembly, we cast thin films of lamellae-forming poly(deuterated-styrene-*block*-methyl

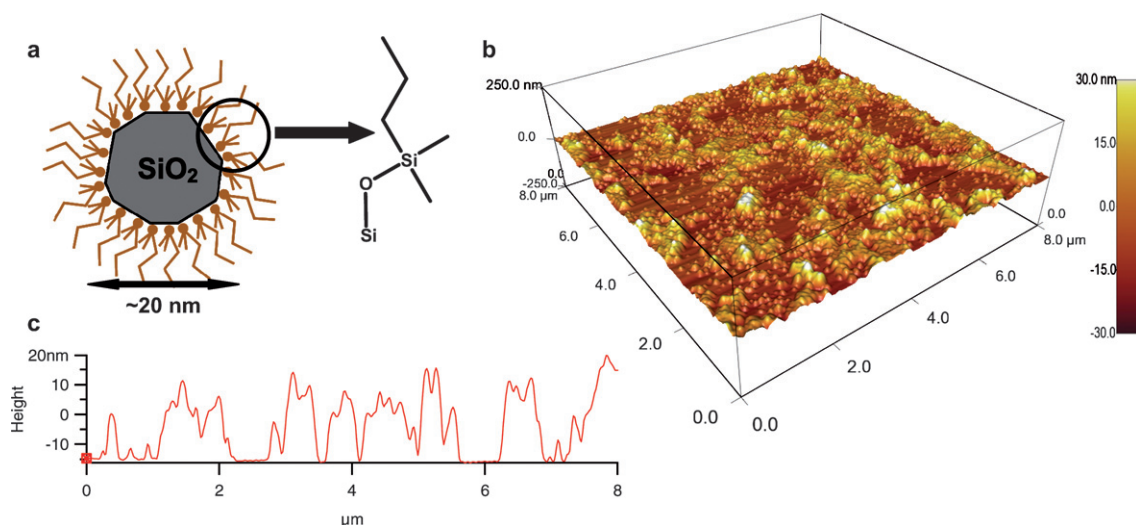


Fig. 1 a, Schematic of the ≈ 20 nm diameter nanoparticles, which have a SiO_2 core coated in a propyl organic ligand. b, Height-mode atomic force micrograph of a silicon wafer with nanoparticles spin-cast to generate roughness. c, Representative cross-section through the AFM height image.

methacrylate) (dPS-PMMA) onto the nanoparticle-treated surfaces. These partially-coated nanoparticle substrates are hierarchically-rough: the rms roughness is 10 nm (as measured by AFM), the 2D areal coverage is 51%, the boundary of the nanoparticles islands has an in-plane fractal dimension of 1.44 ± 0.01 , and the surface topography exhibits a fractal dimension of 2.70 ± 0.09 . To map the behavior of the system, the nanoparticle-treated substrate was exposed to a UV/ozone gradient using an acceleration stage, which resulted in a surface energy gradient (from $\theta_w \approx 50^\circ$ to $\theta_w < 5^\circ$),¹⁹ and the BCP film was cast with a thickness gradient arranged orthogonally to the surface energy gradient.²⁰ Fig. 2a shows an optical image of the thickness gradient after annealing, along with atomic force micrographs (AFMs) of representative surface regions. Some film regions exhibit a fingerprint pattern indicative of a 'vertical' morphology (lamellae sheets perpendicular to the substrate interface), whereas other regions exhibit a uniform surface

indicative of a 'horizontal' morphology (lamellae parallel to substrate). Fig. 2b shows the results of AFM image analysis, quantifying the 'fraction vertical' for a gradient thin film cast on a nanoparticle surface, after 20 h annealing at 165°C , for a substrate region of intermediate oxidation ($\theta_w \approx 37^\circ$). Whereas a film cast on flat silicon would exhibit a fully horizontal state (for any film thickness $> L_0$),²³ the orientation of the film cast on a rough substrate oscillates between a predominantly horizontal state and a predominantly vertical state. The heights of the 'vertical peaks' decrease with increasing film thickness; the horizontal state is ultimately favoured at the free surface of bulk samples. The damping of the peaks with thickness is thus a measure of the spatial influence of the substrate. The spacing between the horizontal regions in Fig. 2b is of the order of $L_0 = 39$ nm, suggesting that these are commensurate regions. The vertical regions can thus be identified as incommensurate film thickness values. We conclude that the nanoparticle-roughened

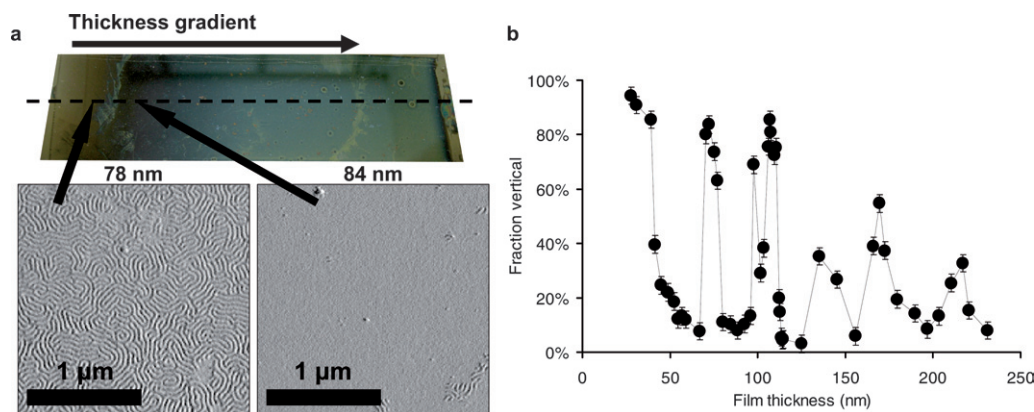


Fig. 2 a, A thickness gradient of a block-copolymer thin film cast onto a nanoparticle-roughened surface exhibits a thickness-dependent morphology. Example phase-mode AFM micrographs show a typical vertically-oriented lamellae region (78 nm film thickness) and a horizontally-oriented region (84 nm) in the same sample. b, By performing image analysis as a function of thickness, a quantitative oscillation between morphologies is evident (measurements taken along the dotted line in (a), a region of partial substrate oxidation, $\theta_w = 37^\circ$). Errors bars represent the standard deviation of repeated measurements; the connecting lines are guides to the eye only.

substrate alters the self-assembly energy landscape, such that it becomes more favourable to form the vertical state, rather than incur the energy penalty required to generate the additional surface area of islands and holes. We note that the nanoparticles become fixed to the substrate during the oxidation step, and do not migrate into the polymer film during casting. This nanoparticle localization was confirmed by AFM and neutron reflectometry. This differentiates the present strategy from previous work on nanoparticle/block-copolymer mixtures,^{10,11} where the nanoparticles were mobile, and segregation (*e.g.* to the substrate interface or the micro-phase boundaries) was dependent on the nanoparticle interactions. Our technique does not fundamentally rely on the use of nanoparticles; they are merely a convenient means of controlling the roughness and average surface energy of the substrate interface. Furthermore, our strategy prevents accumulation of nanoparticles at the free surface, which may be crucial for many applications.

The predominantly horizontal and vertical film regions were nominally flat. However, in the transition zones between these extremes, mixed states with significant height variation developed (Fig. 3a). This lateral partitioning is similar to the formation of islands and holes seen with BCP assembly on flat surfaces, but the height variations do not exhibit the sharp step-heights equal to L_0 which would occur on flat substrates. Instead, rounded droplets appear that correlate with the partitioning between horizontal and vertical morphologies. The correlation between thickness and surface morphology can be made more quantitative by plotting the local morphology as a function of inferred film thickness. That is, by combining the nominal film thickness for a particular film region with the height variation within an AFM image, an absolute height value can be computed for every pixel. Fig. 3b displays this statistical analysis, which includes 2.8×10^7 data points (from 110 AFM images, each containing 512×512 pixels), and computes the relative occurrence of the vertical state for each

thickness range. Importantly, the fact that the oscillations are readily apparent in this data, and are not averaged-out by combining all the AFM images, confirms that the morphology oscillation is strongly sensitive to the *local* thickness. The spacing between the peaks in the data is equal to L_0 , again suggesting that the origin of this oscillation is intrinsic to the BCP assembly, as shown schematically in Fig. 3c.

The internal ordering in the nanostructured films was characterized using rotational small-angle neutron scattering (SANS), where scattering intensity is accumulated as a function of the sample rotation angle. By reorienting the sample, the scattering pattern becomes sensitive to order along different planes through the scattering volume. Fig. 4 shows the reconstructed reciprocal-space scattering intensity maps in a sample coordinate system (the z -axis points along the film normal, and the samples lies in the x - y plane), along with schematics of the inferred order. Fig. 4a shows the scattering for a sample that exhibits the vertical texture by AFM. The scattering map shows a bright peak at $Q_x = 0.16 \text{ nm}^{-1}$, which arises from the lamellar period. The fingerprint patterns observed by AFM cannot distinguish between a vertical state and a cross-section through an entirely random organization, but the SANS enables us to set a bound on the orientation. A sample with lamellae oriented completely randomly would generate a uniform ring of scattering intensity for all $Q = (Q_x^2 + Q_z^2)^{1/2} = 0.16 \text{ nm}^{-1}$. The localization of the peak seen in Fig. 4a indicates that the lamellae are in fact vertically-oriented (within some angular distribution). Fig. 4b shows data for a slightly thicker sample, which exhibits a predominantly vertical surface texture as measured by AFM. The scattering intensity is entirely consistent with AFM, with a slight decrease in the intensity of the peak associated with vertical order. Fig. 4c shows the scattering map for a film of commensurate thickness. For this sample, the peak has nearly completely disappeared, indicating little to no vertical state,

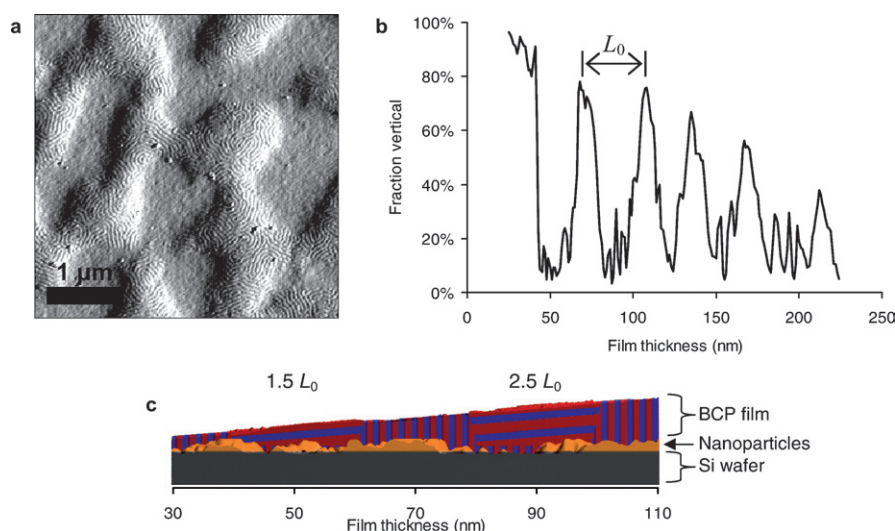


Fig. 3 a, Deflection-mode AFM image (80 nm film) showing local topographic variation, which develops for thickness values between vertical and horizontal regions. Local segregation between vertical and horizontal states correlates with the height variation. b, The local morphology is obtained by averaging the morphology for individual pixels from AFM images, based on inferred thickness. The oscillation between states, with periodicity of L_0 , is evidently a local thickness effect. c, Schematic representation of the oscillation between orientations with changing thickness (the slope of the thickness gradient has been greatly exaggerated). Regions of commensurate thickness, $(n + 1/2)L_0$, generate a horizontal state, whereas incommensurate regions generate a vertical state.

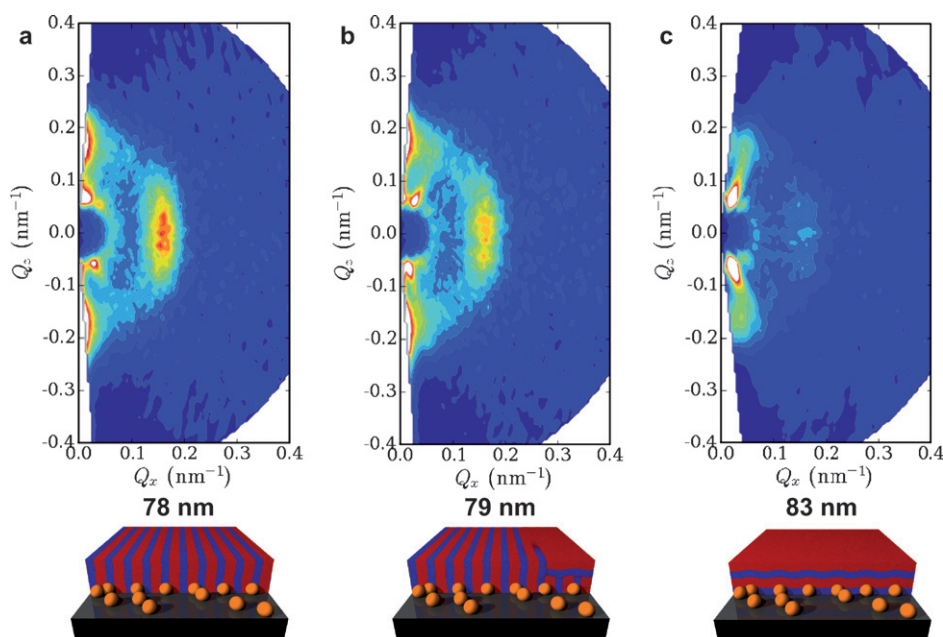


Fig. 4 Small-angle neutron scattering (SANS) data of block-copolymer films assembled on nanoparticle surfaces. The reciprocal-space maps were reconstructed by accumulating SANS data as a function of sample rotation angle. A schematic of the inferred lamellae orientation is provided beneath each map. a, A 78 nm film, which exhibits the vertical morphology by AFM, generates an intense peak at $Q_x = 0.16 \text{ nm}^{-1}$, indicative of vertical order. b, A 79 nm film exhibits a slightly weaker vertical peak. c, The 83 nm film has effectively no peak in the SANS data, consistent with the horizontal morphology observed by AFM.

consistent with a horizontal state as determined by AFM. The rotational SANS data thus confirm the interpretation seen by AFM: that the BCP is sensitive to film thickness, switching between a predominantly horizontal and a predominantly vertical state.

The oxidative treatment of the nanoparticle substrate plays a crucial role in the ordering. By examining the lamellae orientation along the UV/ozone oxidation gradient, we found that the vertical state persists only for intermediate values of oxidation. For both extremely hydrophobic (*e.g.* unoxidized) and extremely hydrophilic (heavily oxidized) surfaces, the vertical state could not be achieved, and uniform horizontal ordering was produced for all thicknesses. This is likely due to the formation of a strong wetting layer (PS on hydrophobic substrates, or PMMA on hydrophilic), which encourages ordering of subsequent horizontal layers. Only when the average surface energy is near ‘neutral’ (where both blocks can wet the interface) is the vertical state energetically accessible.

Finally, we interpret our experimental results by comparing them with the predictions of a free energy model, adapted from Walton *et al.*²⁴ this model considers the relative energy of the horizontal and vertical state in confined lamellae. Cast in a form suitable for our experimental system, it predicts that for asymmetric wetting the free energy difference between the vertical (*v*) and horizontal (*h*) orientations can be given as:

$$\frac{F_h - F_v}{F_0} = \frac{1}{3} \left\{ \lambda^2 + \frac{2}{\lambda} - 3 + \frac{1}{2m\lambda} \left[\delta_k \left(1 - (-1)^{2m} \right) - \delta_1 - \delta_2 \right] \right\} \quad (1)$$

where F_0 is a reference free energy (of an infinitely thick sample), λ is the normalized lamellar spacing (which may deviate slightly

from the bulk equilibrium value), and m is an index related to the number of lamellae (in the equivalent horizontal system). Further, the interfacial energies are included in the δ terms by the relations:

$$\delta_1 = \frac{\gamma_{BS} - \gamma_{AS}}{\gamma_{AB}} \quad (2)$$

$$\delta_2 = \frac{\gamma_{BV} - \gamma_{AV}}{\gamma_{AB}} \quad (3)$$

where γ are the interfacial energies, *A* and *B* refer to the two blocks of the diblock, *S* refers to the substrate, *V* to vacuum/air, and $\delta_k = \delta_2$ if the *B* block is the material that preferentially wets the substrate interface in a conventional antisymmetric horizontal orientation. In the present system, this would be the PMMA block, which has a slight preference for the substrate. In the simplest approximation, the occupation of a given state may be assumed to be $N_i = e^{-F_i/k_B T}$, in which case the relative occurrence of the vertical orientation is:

$$f_v = \frac{N_v}{N_h + N_v} = \frac{1}{e^{-(F_h - F_v)/k_B T} + 1} \quad (4)$$

By combining eqn (1) and (4), we can obtain an estimate of the vertical fraction as a function of thin film thickness (Fig. 5a). The theory captures the primary features of the experimental result: an oscillation between horizontal and vertical states, with a decreasing probability of the vertical state in thicker films. It should be noted that this theory does not explicitly include the surface roughness. However, the roughness of the substrate can in effect be captured in the δ_1 term, since it modifies the effective interaction between the copolymer and the substrate. Thus the primary phenomenological effect of the roughness is to disrupt

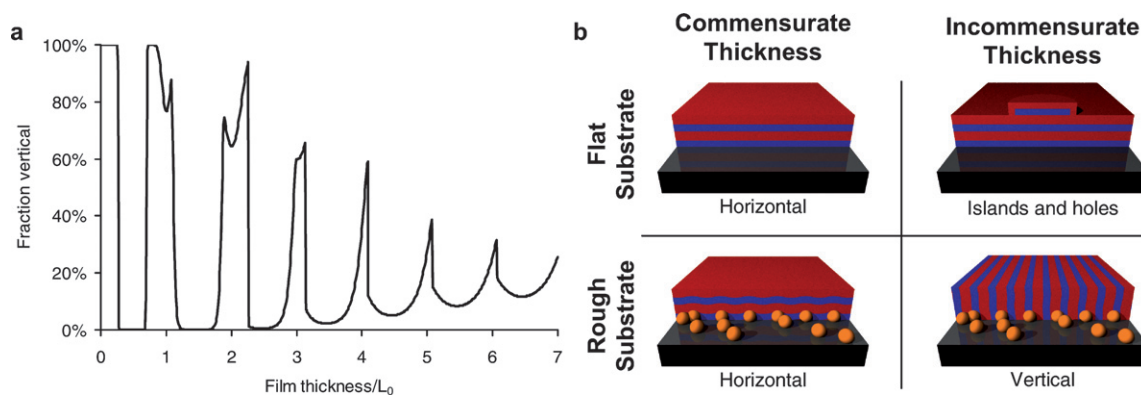


Fig. 5 a, The plot of eqn (4), using values of $\delta_1 = 0.25$, $\delta_2 = \delta_k = -0.3$, and $k_B T/F_0 = 0.007$, shows a distinct oscillation between preferred surface orientations, with a decreasing expression of the vertical state in thicker films. This prediction agrees favourably with the experimental AFM results. b, Schematic of the minimum-energy orientations. Whereas islands and holes form for incommensurate films on flat substrates, the vertical state is instead preferred on rough substrates.

the interfacial wetting. The average surface energy of the interface (experimentally controlled *via* oxidation) would also be included in this term. As shown in Fig. 5b, the energy landscape for lamellae produces islands and holes for incommensurate thicknesses because of the strong preference for a particular block to segregate to the substrate interface. The nanoparticle layer disrupts this interaction, thereby causing the vertical state to be the energy minimum instead. For commensurate thickness, the horizontal state is preferred in both cases. It should be noted, however, that adjustment of other experimental conditions (*e.g.*, annealing temperature) could modify this behavior as well. For the present system, when annealing was performed at 151 °C, a predominantly vertical state was formed for all thicknesses, whereas annealing at 180 °C generated horizontal states for all thicknesses.

Despite the agreement with experiment, the presented theory neglects important aspects of the substrate roughness. In particular, the roughness would impose a bending energy penalty to the horizontal orientation, leading to additional energy terms in eqn (1). Furthermore, the theory assumes rigid top and bottom interfaces, and cannot account for the experimentally observed formation of surface height variations for the mixed states. Some theoretical treatments have analyzed the effect of substrate roughness on the self-assembly of block-copolymers,^{25–27} and show qualitative agreement with the results shown here, where substrate surface topography destabilizes the horizontal state. However the presented theories model roughness as a simple periodic function, whereas the experimental roughness is random and hierarchical. Thus the theoretical sensitivity to the length-scale of the corrugation is not observed in the experimental system, since it contains roughness at many different length-scales. The theoretical work of Balazs and coworkers^{28,29} for nanoparticle/block-copolymer mixtures is also relevant. Although the present system does not have the nanoparticle mobility that was modeled in that work, a comparison is still instructive. In the nanoparticle/block-copolymer mixtures, qualitatively similar ordering is observed, with an oscillation in free energy, as a function of confinement size, which causes the parallel and perpendicular states to be alternately the energy minimum. The models predict that, under certain circumstances,

the nanoparticles will segregate to the film-substrate interface, modifying the interaction in a similar way to the substrate preparations presented here.

A consequence of the hierarchical roughness is that the self-assembly was relatively insensitive to the substrate preparation (*e.g.*, spin-casting solution concentration and spin-coating speed could be changed by a factor of two without affecting the results). More significantly, it was found that the combination of controlling surface energy and surface roughness makes the assembly less sensitive to either effect. Experiments of block-copolymer assembly on statistical random copolymer substrates^{7,30} showed that the vertical state formed only a narrow range of surface compositions, corresponding to a water contact angle range of $\approx 4^\circ$. In the present system, the gradient in surface energy allowed us to probe the sensitivity to this parameter, where we observed a significant vertical state ($>80\%$) for $20^\circ < \theta_w < 50^\circ$. This $\approx 30^\circ$ range for the surface energy tolerance is a lower-bound, since the samples studied here exhibited a maximum contact angle of 50° due to the partial substrate exposure inherent to the high-roughness assembly. It is likely that the vertical state would persist to $\theta_w \approx 80^\circ$. Imperfections in the formation of the rough interface and the oxidation treatment do not impact the assembly behavior. This effect is due both to the intrinsically defective interface generated by the nanoparticles, and due to the inherent nature of self-assembly, which seeks to find a defined energy minimum despite imperfections, and thereby heals over defects. Thus, while the assembly is clearly influenced by both substrate roughness and surface energy, it is relatively insensitive to changes in either parameter.

Conclusions

In conclusion, we have described a new general strategy for controlling the properties of coatings in a robust fashion, whereby self-assembly is combined with an inherently defective interface in order to select a desired morphology and/or orientation. In particular we propose tunable nanoparticles as a convenient means of preparing such surfaces, since the dual control of roughness and surface energy enables one to select a region of parameter space that is insensitive to either

parameter. We have shown that morphology transitions can be accessed by tuning the film-substrate interaction. In the case of block-copolymer lamellae, we have shown that a theoretically-predicted, but previously unobserved, oscillation between horizontal and vertical orientations can be achieved in a single sample. The observed random in-plane order achieved in the vertical states may be acceptable in some applications (e.g. controlling chemical surface-expression in coatings), but may not be in others (e.g. lithography). It is thus worth noting that this strategy could be combined with other directed assembly techniques, such as electric fields, topographical or chemical patterns, or directional thermal fronts. It is anticipated that this assembly strategy will generalize to many other systems (polymer blends, liquid crystals, etc.). From an industrial standpoint, the ability to bias self-assembly without resorting to costly and stringent techniques (e.g. lithography or other clean-room procedures) would be of considerable utility. In fact, the vast majority of commonly occurring surfaces (in everyday life, as well as in industrial processing) are neither flat nor regularly patterned, but rather exhibit micro-scale and nano-scale roughness. Thus our intentionally rough surface treatment provides insight into how common rough surfaces can be utilized to select a desired self-assembled order.

Acknowledgements

K.G.Y. acknowledges the support of NSERC Canada in the form of a Postdoctoral Fellowship. We thank the NIST Center for Neutron Research for providing facility access for SANS measurements, and recognize Paul Butler and Ronald Jones for contributions to SANS data acquisition. Additionally, Michael J. Fasolka and Christopher M. Stafford are acknowledged for their help with the combinatorial techniques, and Jack Douglas for helpful discussions.

References

- 1 M. J. Fasolka and A. M. Mayes, *Annual Review of Materials Research*, 2001, **31**, 323–355.
- 2 B. Ashok, M. Muthukumar and T. P. Russell, *J. Chem. Phys.*, 2001, **115**, 1559–1564.
- 3 G. G. Pereira and D. R. M. Williams, *Macromol.*, 1999, **32**, 8115–8120.
- 4 Y. Tsori and D. Andelman, *Macromol.*, 2002, **35**, 5161–5170.
- 5 X. M. Yang, R. D. Peters, P. F. Nealey, H. H. Solak and F. Cerrina, *Macromol.*, 2000, **33**, 9575–9582.
- 6 S. Ouk Kim, H. H. Solak, M. P. Stoykovich, N. J. Ferrier, J. J. de Pablo and P. F. Nealey, *Nature*, 2003, **424**, 411.
- 7 P. Mansky, T. P. Russell, C. J. Hawker, M. Pitsikalis and J. Mays, *Macromol.*, 1997, **30**, 6810–6813.
- 8 P. Mansky, T. P. Russell, C. J. Hawker, J. Mays, D. C. Cook and S. K. Satija, *Phys. Rev. Lett.*, 1997, **79**, 237.
- 9 E. Huang, L. Rockford, T. P. Russell and C. J. Hawker, *Nature*, 1998, **395**, 757.
- 10 Y. Lin, A. Boker, J. He, K. Sill, H. Xiang, C. Abetz, X. Li, J. Wang, T. Emrick, S. Long, Q. Wang, A. Balazs and T. P. Russell, *Nature*, 2005, **434**, 55.
- 11 S. W. Hu, W. J. Brittain, S. Jacobson and A. C. Balazs, *European Polymer Journal*, 2006, **42**, 2045–2052.
- 12 E. Sivaniah, Y. Hayashi, S. Matsubara, S. Kiyono, T. Hashimoto, K. Kukunaga, E. J. Kramer and T. Mates, *Macromol.*, 2005, **38**, 1837–1849.
- 13 Y. Tsori, E. Sivaniah, D. Andelman and T. Hashimoto, *Macromol.*, 2005, **38**, 7193–7196.
- 14 E. Sivaniah, Y. Hayashi, M. Iino, T. Hashimoto and K. Fukunaga, *Macromol.*, 2003, **36**, 5894–5896.
- 15 Certain equipment, instruments or materials are identified in this paper in order to adequately specify the experimental details. Such identification does not imply recommendation by the National Institute of Standards and Technology nor does it imply the materials are necessarily the best available for the purpose.
- 16 D. A. Savin, J. Pyun, G. D. Patterson, T. Kowalewski and K. Matyjaszewski, *J Polym Sci Pol Phys*, 2002, **40**, 2667–2676.
- 17 J. T. Han, S. Kim and A. Karim, *Langmuir*, 2007, **23**, 2608–2614.
- 18 C. Douketis, Z. H. Wang, T. L. Haslett and M. Moskovits, *Phys Rev B*, 1995, **51**, 11022–11031.
- 19 B. C. Berry, C. M. Stafford, M. Pandya, L. A. Lucas, A. Karim and M. J. Fasolka, *Rev Sci Instrum*, 2007, **78**, 072202.
- 20 C. M. Stafford, K. E. Roskov, T. H. Epps and M. J. Fasolka, *Rev Sci Instrum*, 2006, **77**, 023908.
- 21 C. Harrison, Z. Cheng, S. Sethuraman, D. A. Huse, P. M. Chaikin, D. A. Vega, J. M. Sebastian, R. A. Register and D. H. Adamson, *Phys. Rev. E*, 2002, **66**, 011706.
- 22 The data in this manuscript, and in the figures, are presented along with the standard uncertainty involved in the measurement, where the uncertainty represents one standard deviation from the mean.
- 23 M. J. Fasolka, P. Banerjee, A. M. Mayes, G. Pickett and A. C. Balazs, *Macromol.*, 2000, **33**, 5702–5712.
- 24 D. G. Walton, G. J. Kellogg, A. M. Mayes, P. Lambooy and T. P. Russell, *Macromol.*, 1994, **27**, 6225–6228.
- 25 M. S. Turner and J. F. Joanny, *Macromol.*, 1992, **25**, 6681–6689.
- 26 Y. Tsori and D. Andelman, *Macromol.*, 2003, **36**, 8560–8566.
- 27 I. Podariu and A. Chakrabarti, *J. Chem. Phys.*, 2000, **113**, 6423.
- 28 J. Y. Lee, Z. Y. Shou and A. C. Balazs, *Macromol.*, 2003, **36**, 7730–7739.
- 29 J. Y. Lee, Z. Shou and A. C. Balazs, *Phys. Rev. Lett.*, 2003, **91**.
- 30 P. Mansky, Y. Liu, E. Huang, T. P. Russell and C. Hawker, *Science*, 1997, **275**, 1458–1460.